Spinal neural tube formation and regression in human embryos

Chloe Santos *, Ailish Murray [1]*, Abigail R. Marshall *, Kate Metcalfe, Priyanka Narayan, Sandra C. P. de Castro, Eirini Maniou, Nicholas D. E. Greene, Gabriel L. Galea and Andrew J. Copp [2]

Developmental Biology & Cancer, UCL Great Ormond Street Institute of Child Health, 30 Guilford Street, London WC1N 1EH, UK

* These authors contributed equally to the study

[1] Current address: Moorfields Eye Charity, 162 City Road, London, EC1V 2PD

[2] Author for correspondence: tel: +44 207 905 2355; e-mail: a.copp@ucl.ac.uk

ABSTRACT

Formation of the nervous system in the human spinal region involves primary and secondary neurulation, in which the neural tube forms by closure and canalisation respectively. These processes are incompletely understood, in part due to the challenge of accessing human embryos at 3-7 weeks post-conception. A growing effort is being made to recapitulate events of neurulation in organoids derived from human stem cells. Here we present findings from a series of human embryos that can provide 'normative data' for interpretation of organoid results. The primary neural tube shows progressive closure during Carnegie Stages (CS) 10-13, with completion at the 30 somite stage. Somites form every 7 h, compared with organoid findings that indicate a 5 h 'segmentation clock'. Human neural plate bending morphogenesis is closely similar to that in mouse embryos. Secondary neurulation begins from CS13, with initial formation of a single lumen as in mouse, not by coalescence of multiple lumens as in chick. Termination of axial elongation occurs after downregulation of *WNT3A* and *FGF8* in the CS15 embryonic tailbud, with a 'burst' of apoptosis that may remove the neuro-mesodermal progenitors. Axial length declines during tail regression, with different axial elements showing varied patterns of apoptotic removal.

INTRODUCTION

Development of the lumbosacral spinal cord is a critical period of embryogenesis. Not only does motor control and sensation in the legs and lower body depend on this event, but proper functioning of bladder, rectum and genital organs are all critically dependent on nerves arising from the low spinal cord. A major group of congenital malformations termed neural tube defects (NTDs) result when low spinal neurulation fails to be completed or is otherwise abnormal, and these can be open or closed (skin-covered) lesions.

Open spina bifida (also called myelomeningocele) results from defective closure of the primary neural tube, most often at lumbar and upper sacral levels, leading to a neurodegenerative defect that is disabling in most individuals (Copp et al., 2015). Closed ‘dysraphic’ conditions arise at lower sacral and coccygeal levels of the body axis and result from disturbance of secondary neurulation, in which the neural tube forms by a process of canalisation, without formation of neural folds. Dysraphic conditions involve an abnormal anatomical relationship between secondary neural tube and surrounding tissues, often with ectopic adipose tissue, as in spinal lipoma and lipomyelomeningocele (Jones et al., 2019). Closed dysraphism may be asymptomatic, but significant disability can occur through tethering of the low spinal cord to non-neural tissues (Agarwalla et al., 2007).

Primary and secondary neurulation have been studied extensively in experimental animals, especially chick, mouse and rat. Despite the relative inaccessibility of neurulation-stage human embryos (3 to 6 weeks post-conception), a number of studies have described the anatomical, histological and ultrastructural features of secondary neurulation (Table S1). Although limited molecular research has been performed: e.g. to determine the mode of cell death in human tail regression (Vilovic et al., 2006), a few studies have begun to address gene expression during human secondary body development (Krupp et al., 2012; Olivera-Martinez et al., 2012).

Caudal development comprises not only formation of the secondary neural tube, but also other tissue types within the ‘secondary body’ region. This part of the body axis – beyond the cloacal plate which marks the future anus – includes the secondary notochord, tail somites, caudal vessels, tail-gut and surrounding surface ectoderm (future epidermis). These structures show marked tissue-to-tissue variation in development. For example, tail regression in human embryos involves loss of all tail components, whereas the rodent tail maintains the somites and notochord, but loses the secondary neural tube and tail-gut. The regulation of this balance between maintenance and loss of tail structures is not understood.

A related area of interest is the molecular control of axial elongation. A population of self-renewing stem cells, termed neuro-mesodermal progenitors (NMPs), resides in the caudal-most embryonic region (the tailbud), with NMPs giving rise to neural and mesodermal derivatives, including the secondary neural tube and somites (Henrique et al., 2015). NMP maintenance is required for axial elongation, and an interplay between WNT3A and FGF8 expression, which promote NMP survival in the tailbud, and endogenous retinoic acid which promotes differentiation, regulates body length (Wilson et al., 2009).

In the present study, we examined caudal development in 102 human embryos, at Carnegie Stages (CS)10-18 (3.5 to 6.5 weeks post-conception). The aim was to gain new information on several unanswered or controversial questions in human neurulation, including: (i) how the embryo transitions from primary to secondary neurulation; (ii) the mode of formation of the secondary neural tube; (iii) the rate of somite formation during low spinal development; (iv) the possible roles of WNT3A and FGF8 in regulating axial elongation; (v) whether a ‘burst’ of apoptosis coincides with termination of axial elongation. A further aim was to gather and present findings on human spinal neurulation that can serve as ‘normative data’ to aid interpretation of research involving multicellular ‘organoid’ structures, that are being increasingly used to model various aspects of human axial development (Amadei et al., 2022; Denham et al., 2015; Fedorova et al., 2019; Karzbrun et al., 2021; Libby et al., 2021; Moris et al., 2020; Rifes et al., 2020).

RESULTS

The study involved 102 human embryos (Table 1), obtained from the MRC/Wellcome Human Developmental Biology Resource (www.hdbr.org), with UK ethics committee approval. Embryos were donated by women undergoing termination of pregnancy for 'social' reasons, in most cases by mifepristone/misoprostol-induced (medical) delivery, with a few embryos obtained by ultrasound-guided vacuum aspiration (surgical). All embryos in the study had a normal karyotype and external morphology, and were assigned to Carnegie Stages (CS), as described (Bullen and Wilson 1997; O'Rahilly and Muller 1987). Comparisons to mouse were with random-bred CD1 embryos, staged by embryonic (E) day, where E0.5 is the day following overnight mating.

Morphology of human PNP closure

Relatively few human embryos with an open PNP have been reported in the literature (Müller and O'Rahilly 1987; O'Rahilly and Müller 2002), probably owing to the early stage at which primary neurulation is completed (end of week 4, post-conception). In two intact CS12 embryos (Figure 1A,B; crown-rump length: 3 mm; 22-23 somites), we identified an open PNP by microscopic inspection at collection (Figure 1C,D). Transverse histological sections confirmed an open neural tube in the caudal region, with minimal tissue damage evident, indicating that primary neurulation was not yet complete. The neural plate is relatively flat in the most caudally located sections, although incipient dorsolateral hinge points (DLHPs) are visible (Figure 1E,F). The notochord underlies the neural plate midline, and the caudal end of the hindgut is visible beneath the notochord in one embryo (Figure 1E), but not the other (Figure 1F). In more rostral sections, close to the 'zippering' point of PNP closure, elevated neural folds flank a marked ventral midline bend in the neural plate, the median hinge point (MHP), which precisely overlies the notochord (Figure 1G,H). DLHPs are also clearly present, unilaterally in one embryo (Figure 1G) and bilaterally in the other (Figure 1H). As in the mouse (McShane et al., 2015), the DLHPs are situated where the neural plate changes from basal contact with surface ectoderm to basal contact with paraxial mesoderm. We conclude that both MHP and DLHPs characterise PNP closure in human embryos

at CS12, marking a direct equivalence to Mode 2 spinal neurulation in the mouse (Shum and Copp 1996).

Timing of human PNP closure

PNP length data were obtained from a series of photographic images of CS10-CS13 embryos (n = 40). To allow for differences in overall embryonic size, PNP measurements were normalised to the length of a recently formed somite in the same embryo (Figure 1C). The plot of PNP length/somite length against somite number shows a steady decline in the length of open neural folds in the caudal region, until 6/12 embryos at CS13 have completely closed, while most of the others show a very small PNP. There were no obvious differences in closure rate or timing between female (n = 24) and male (n = 16) embryos. Hence, PNP closure in human embryos occurs around the 30 somite stage, as also reported for outbred mouse strains (Copp et al., 1982).

Development and regression of the human embryonic tail

Caudal development was studied in 37 human embryos (CS13 to CS18), which covered the period 28-45 days post-conception (Table 2; Figure 2A,B,I). Crown-rump length increased 2.5-fold during this period, from a mean value of 6.4 mm at CS13 to 15.4 mm at CS18 (Table 2; Figure 2K). Observations on the intact embryos showed that the PNP is closed in most embryos by CS13, and a developing tailbud is present which exhibits mild ventral curvature and a thick rounded tip (Figure 2C). Somites are visible proximal to the tailbud (arrowheads in Figure 2C), with an intervening region of presomitic mesoderm at CS13 (yellow bracket in Figure 2C). By CS16, however, the somites extend almost to the tail tip (yellow arrow in Figure 2F). As development progresses, striking changes occur in the tail which continues to lengthen (Table 2) but simultaneously narrows, particularly at the tip, to yield a sharply pointed structure by CS16 (Figure 2D-F). At the same time, the tail straightens and even becomes dorsally bent (Figure 2F). Subsequent to CS16, the tail shortens (Figure 2G; Table 2), and its distal portion becomes increasingly translucent in appearance. By CS18, only a short, curved stump remains (Figure 2H), and the tail is lost completely thereafter.

Somite formation

Between CS10 and CS13, during PNP closure (Figure 1I), somite number increases approximately linearly with days of gestation (Figure 1J): mean (± SD) somite numbers were: 8.0 ± 1.4 at CS10, 18.4 ± 2.6 at CS11, 23.5 ± 3.4 at CS12 and 30.0 ± 2.8 at CS13. Hence, 20 somites are added over a 6-day period, equating to the formation of 3.4 somites per gestational day, or a new somite every ~7 h. This compares with a 5 h periodicity observed for the human 'in vitro segmentation clock' in stem cell-derived presomitic mesoderm-like cells (Diaz-Cuadros et al., 2020; Matsuda et al., 2020). Following PNP closure at CS13, the largest somite number was at CS16 (36.6 ± 1.2; Table 2), although there was no statistically significant increase between CS13 and CS16 (Figure 2J). By CS17 and 18, we could identify only 31-34 somites, a significant reduction in number (Figure 2J), suggesting that shortening of the tail during regression involves loss of somites (Table 2).

Mode of cell death during tail regression

Transverse histological sections through human and mouse embryonic tails were processed for immunohistochemistry using anti-activated caspase 3. Stained cells were readily identified in the tails of both species (Figure 3), arguing for a role of caspase-dependent apoptosis during tail regression in human and mouse. Principal sites of apoptotic cell death include the regressing tail-gut (Figure 3A-C,G,I), secondary neural tube (Figure 4H) and, most abundantly, the ventral mesoderm overlying the epithelial ventral ectodermal ridge (Figure 3C,H,I). Proliferative cells, detected by phospho-histone H3 immunostaining, co-exist with apoptotic cells in the human secondary neural tube (Figure 4I). We also detected TUNEL-positive cells in both mouse (Figure 3A,D,E) and human tail sections (not shown), further confirming the presence of apoptotic cells during tail development/regression.

Regression of the tail-gut proceeds from rostral to caudal in human and mouse

While the human embryonic tail appears to regress from caudal to rostral (Figure 2), the proximal part of the tail-gut has been found to degenerate before the distal part in both rat (Butcher 1929; Qi

et al., 2000) and mouse (Nievelstein et al., 1993). We confirmed this finding, by analysis of serial tail sections in mouse and human embryos. For example, Figure 3D shows a proximal section through a mouse tail at E12.5 in which there is no discernible gut epithelium or lumen. A blood vessel is positioned where the tail-gut would normally be found. In contrast, a more distal section through the same tail reveals a gut epithelium with lumen (Figure 3E). A similar finding was obtained from the human embryos: a proximal section at CS13 demonstrates lack of tail-gut (Figure 3F) but a more distal section of the same tail shows a tail-gut, containing apoptotic cells (Figure 3G). We conclude that rostral-to-caudal loss of tail-gut is a general finding among mammalian embryos.

A burst of apoptosis at cessation of tail elongation

We observed enhanced apoptosis in the mouse tailbud at E13.5 (Figure 4B), compared with E13.0 and E14.0 when relatively few dying cells were present (Figure 4A,C). Similarly, in sections through the caudal-most region of human embryos, apoptosis was not observed at CS13 (Figure 4D), became intense at CS15 (Figure 4E), and diminished in intensity by CS18 (Figure 4F). Hence, in both mouse and human tails, there appears to be a 'burst' of apoptosis at the stage when tail growth ceases, and just before regression of internal structures gets underway.

Expression of *FGF8* and *WNT3A* during human tailbud elongation

To begin an assessment of the mechanisms that may regulate elongation of the human embryonic tail, and its cessation, we performed whole mount in situ hybridisation for *FGF8* and *WNT3A* (n = 2 embryos minimum for each gene at each stage). These genes are developmentally regulated during axial elongation in chick and mouse embryos, with strong expression in the tailbud during elongation, and down-regulation before axial growth ceases. Direct inactivation or indirect down-regulation of the genes leads to premature axial truncation (Wilson et al., 2009).

In accordance with these findings, we observed strong expression of *FGF8* in the tailbud at CS12 and CS13, as revealed in whole embryos (Figure 5A, B) and longitudinal sections through

hybridised caudal regions (Figure 6A, B). At CS14, *FGF8* expression reduced dramatically so that only a small 'dot' of expression was detected in the tailbud (Figures 5C, 6C), and by CS15 expression of *FGF8* was no longer detectable in the tail (Figures 5D, 6D). Expression of *WNT3A* followed a similar pattern with strong expression in the tailbud at CS12 (Figures 5E, 6E), reduced expression intensity at CS13 (Figures 5F, 6F), a remaining 'dot' of tailbud expression at CS14 (Figures 5G, 6G), and no detectable *WNT3A* expression in the tail at CS15 (Figures 5H, 6H). We conclude that expression of *FGF8* and *WNT3A* mirrors the relationship seen in mouse and chick, with strong tailbud expression during active axial extension, and dramatic down-regulation of both genes before the onset of axial growth cessation. It is striking that down-regulation appeared complete by CS15, even though the embryonic tail does not reach its maximum length until some days later, at CS16 (Table 2). Down-regulation of *Fgf8* and *Wnt3a*, well in advance of cessation of axial elongation, has also been observed in mouse embryos (Cambray and Wilson 2007).

Mode of secondary neural tube formation in human embryos

In our study of tail morphology (Figures 3 and 4), fifteen human embryonic tails were initially sectioned and stained, of which six had a neural tube with only a single lumen whereas nine showed evidence of multiple lumens in some transverse sections. This confirms previous findings of multiple neural tube lumens in human embryonic tails (Bolli 1966; Lemire 1969; Saitsu et al., 2004). We identified at least two, and sometimes more, neural tube profiles in a single transverse section (e.g. at CS15; Figure 4G-I). The pattern and extent of neural tube duplication varied between embryonic tails, with multiple lumens along much of the tail length in some, but only at particular axial levels in others. Interestingly, a single lumen was invariably noted in the distal-most portion of the neural tube, closest to the tailbud tip (e.g. at CS13-CS18; Figure 4D-F), whereas multiple lumens were generally found at more rostral levels of the embryonic tail (Figure 4G-I).

This finding called into question the suggestion (Figure 7A) that multiple neural tube lumens represent a mode of human secondary neurulation similar to that seen in the avian embryo (Lemire 1969; Pang 2020; Saitsu et al., 2004). In chick, multiple lumens form distally in the tail bud, and

coalesce more rostrally to form the secondary neural tube (Criley 1969; Schoenwolf and De Longo 1980; Yang et al., 2003). An alternative view is that multiple lumens arise only later in human secondary body formation (Catala 2021), perhaps representing splitting of the secondary neural tube in relation to ongoing tail regression (Figure 7B). To help resolve this issue, five further human embryonic tails (CS17) were sectioned serially, with careful examination of the entire tail axis for secondary neural tube status. Multiple secondary neural tube lumens were visible in three of the embryos (Figure 7C-E,F-H), but not in the others (Figure 7I-K). Importantly, none of the embryos showed evidence of multiple lumens at tail-bud level (Figure 7C,F,I), where the secondary neural tube is formed initially. We conclude that multiple neural tube lumens in human embryonic tails represent splitting, which tends to occur rostrally and does not represent a secondary neurulation mechanism involving coalescence of multiple lumens, as in chick. Humans therefore resemble other mammals in initially forming a single neural tube lumen in the tail-bud.

DISCUSSION

The development and later disappearance of the human tail has been of interest to embryologists for more than a century (Catala 2021). To better appreciate the knowledge base for human embryonic caudal development, we conducted a systematic literature review using several search terms (see Materials and Methods). This generated a long-list of publications that was filtered to include only those with primary data relating to caudal development in human embryos. The final list comprises 25 papers (Table S1) that span 100 years of research, from the early 1900s (Kunitomo 1918; Streeter 1919) to recent times (Tojima et al., 2018). This research was based on at least 777 human embryos obtained from varying sources (Table S1) including induced termination of pregnancy for 'social' reasons (where most embryos are expected to be normal), as well as spontaneous abortion (miscarriage) and ectopic pregnancy, where embryonic abnormalities are likely to be frequent. Hence, interpretation of embryo morphology in these studies needs to take into account the mode of procurement of the human specimens.

Several aspects of caudal development are addressed by the studies in Table S1. These include: completion of primary neurulation with PNP closure, the transition into secondary neurulation, the mode of formation and regression of the secondary neural tube, the observation of multiple neural tube lumens, the formation and regression of somites, notochord and gut in the tail region, the role of programmed cell death in tail regression, and initial studies of gene expression in the caudal region of human embryos. Taken together with the findings of the present study, this accumulated literature provides a strong morphological evidence base for 'in vivo' human caudal development, against which in vitro studies can be judged in the emerging field of stem cell-derived organoid differentiation. The latter is producing multicellular structures that may ultimately provide experimentally tractable models for some aspects of human axial development (Amadei et al., 2022; Denham et al., 2015; Fedorova et al., 2019; Karzbrun et al., 2021; Libby et al., 2021; Moris et al., 2020; Rifes et al., 2020).

Concept of a human 'tail'

The human tail develops and then regresses during weeks 4-7 post-conception and is composed of a secondary neural tube, notochord, somites and tail-gut, with undifferentiated mesenchyme at its tip (the tailbud or 'caudal eminence'), all within a surface ectoderm covering. Since it never becomes vertebrated, in contrast to the tails of most other mammals, some authors consider the human caudal appendage does not qualify as a 'tail' (Müller and O'Rahilly 2004). On the other hand, the presence of caudal somites with vertebra-forming potential are considered by other authors to endow the human caudal appendage with all the hallmarks of a mammalian tail (Kunitomo 1918). In keeping with common usage, we have referred to the transient human caudal appendage as a tail in this paper.

Mode of development of the human secondary neural tube

Secondary neurulation in mouse and rat involves formation of a single 'rosette' structure caudally, in which cells aggregate ('condense') from the dorsal tailbud mesenchyme, with subsequent (more rostral) organisation of the cells around a single lumen. This process is driven by apical junction formation, not by cell death (Butcher 1929; Kostovic-Knezevic et al., 1991; Nievelstein et al., 1993; Schoenwolf 1984). In chick, by contrast, a caudal-to-rostral sequence of events occurs in which several independent lumens arise in the dorsal tailbud mesenchyme and, at more rostral levels, these coalesce to form the secondary neural tube (Criley 1969; Schoenwolf and De Longo 1980; Yang et al., 2003). Coalescence is a cell intercalation process driven by TGFβ/SMAD3 signalling (Gonzalez-Gobartt et al., 2021).

The mode of formation of the human secondary neural tube is controversial. Multiple neural tube lumens have often been observed in the developing or regressing tail (Bolli 1966; Fallon and Simandl 1978; Hughes and Freeman 1974; Lemire 1969; Pytel et al., 2007; Saitsu et al., 2004; Yang et al., 2014), whereas other studies identify only a single lumen (Müller and O'Rahilly 1987; Nievelstein et al., 1993). Here, we found multiple secondary neural tube lumens in some but not all human embryos. An important question is whether such multiple lumens are part of the normal

secondary neurulation process in humans – thus making the human more similar to chick than mouse, as has been claimed (Pang 2020). Alternatively, multiple lumens could arise through later ‘splitting’ of the previously formed neural tube. In mice, neural tube duplication is part of several mutant phenotypes and, when present, is a sign of pathology (Cogliatti 1986).

A limitation of previous studies is the paucity of information on the morphology of the secondary neural tube at precise rostro-caudal axial levels. To shed light on this question, we examined human embryonic tails with the specific aim of determining the axial sequence of secondary neurulation events. Our findings show that multiple lumens, if present, feature at relatively rostral (mature) levels of the secondary neural tube and are absent from the most caudal (immature) levels, close to the tailbud. This applies to embryos early (e.g. CS13) and late (e.g. CS17) in the secondary neurulation process, and argues strongly against coalescence of chick-like multiple lumens as a feature of normal human secondary neurulation. A recent review has drawn the same conclusion (Catala 2021). Hence, ‘splitting’ of the human secondary neural tube appears a common but not obligatory phenomenon, likely reflecting changes related to tail regression.

Tail-gut: origin and mode of regression

The tail-gut is an extension of the hindgut, beginning caudal to the level of the cloacal plate (future anus), which is located ventral to somite 29 in the mouse (Nievelstein et al., 1993). The tail-gut forms and then regresses in both tailed (mouse, rat) and non-tailed (chick, human) animals. Interestingly, human tail-gut loss has been described as involving rostral-to-caudal degeneration rather than a more intuitive caudal-to-rostral loss (Fallon and Simandl 1978; Kunitomo 1918). Consistent with this, the tail-gut lumen persists longest at the tail tip in rat (Butcher 1929; Qi et al., 2000) and mouse (Nievelstein et al., 1993). Our findings confirm that the tail-gut is lost at rostral before caudal levels in both human and mouse embryos.

In contrast to the consensus on tail-gut regression, there is disagreement over the developmental origin of the tail-gut. Anatomical and histological studies in rat, mouse and human often conclude

that the tail-gut originates by mesenchyme-to-epithelium transition of tailbud cells, in a manner similar to the origin of the secondary neural tube (Gajovic et al., 1989; 1993; Nievelstein et al., 1993; Svajger et al., 1985). However, others consider the tail-gut to arise by caudally directed extension of the hindgut (Jolly and Ferester-Tadie 1936). Grafting of the E10.5 mouse tailbud beneath the kidney capsule produced no evidence of gut epithelial differentiation, in contrast to primitive streak/tailbud fragments at E8.5 and E9.5 which regularly produced this derivative. This finding is consistent with loss of gut-forming potential in the later stage tailbud (Tam 1984).

The question of tail-gut origin can also be considered in light of the identification of NMPs: the stem cell population in the tailbud for tissues of the caudal embryonic region (Wilson et al., 2009; Wymeersch et al., 2021). A retrospective clonal analysis found gut endoderm only as part of rostrally-derived clones, unlike neural tube and paraxial mesoderm that were represented in clones extending into the tailbud at E10.5 (Tzouanacou et al., 2009). This led to the idea that NMPs are bipotential, forming neural and paraxial mesodermal derivatives, whereas the endodermal lineage is set aside separately, early in gastrulation. These findings are consistent with results of DiI-based lineage tracing and tissue grafting experiments (Cambray and Wilson 2002; 2007) which show that the NMP population at the chordoneural hinge region (CNH) of the tailbud is fated to form neural and mesodermal derivatives, but not tail-gut. It remains to be determined, therefore, how the tail-gut is formed during secondary body development. For example, we do not understand the location and nature of the progenitor population that allows tail-gut formation to ‘keep pace’ with formation of the neural tube, paraxial mesoderm and notochord during axial elongation. Moreover the tissue continuity between the caudal end of the tail-gut and the mesenchyme of the tail bud (Gajovic et al., 1989; 1993; Nievelstein et al., 1993; Svajger et al., 1985) remains unexplained.

Mechanism of cessation of tail elongation

Termination of axial elongation is highly species-specific, occurring in embryos with fewer than 40 somites in human (Table 2), at ~ 52 somite stage in chick, and in embryos with 65 somites in rat and mouse (Olivera-Martinez et al., 2012). One question is whether the underlying molecular and

cellular mechanisms are shared, despite these variations in timing, or are fundamentally different between species. Our findings with human embryos support a shared mechanism, as we find that expression of *FGF8* and *WNT3A* are developmentally regulated in close relationship to the time-course of axial elongation, similar to that in rodent embryos. Moreover, cessation of tail growth in the mouse has been linked to a burst of apoptosis in the tailbud around E13.5 (Wilson et al., 2009), and we detected an analogous burst of apoptosis in the CS15 human tailbud. Hence, a similar mechanism may underlie growth termination of the much shorter human embryonic tail.

Type and timing of cell death during tail regression

While programmed cell death is recognised to participate in tail regression, the precise mode of cell death has been debated. In immunohistochemistry studies, it was concluded that apoptosis occurs only in the human cranial embryonic region, and non-apoptotic ('necrotic-like') death of tail structures was identified in the regressing human tail (Sapunar et al., 2001; Vilovic et al., 2006). In contrast, cell death during chick tail regression was shown to involve caspase-dependent apoptosis (Miller and Briglin 1996). Using anti-caspase 3 and TUNEL methods, we identified apoptosis in the human tail, with patterns of cell death occurring in a closely similar way between human and mouse embryos. We conclude that caspase-dependent apoptosis is the predominant mode of cell loss during tissue regression in the tails of both mouse and human.

MATERIALS AND METHODS

Human embryos

All embryos were obtained from the MRC/Wellcome Human Developmental Biology Resource (HDBR; www.hdbr.org) with UK ethics committee approval and written consent of donors. Embryos were collected on ice in L-15 medium, rinsed in phosphate buffered saline (PBS) and fixed overnight at 4°C in 4% paraformaldehyde (PFA) in PBS. Only embryos that had normal external morphology and a normal karyotype were included in the study.

Mouse embryos

Mouse studies were conducted under auspices of the UK Animals (Scientific Procedures) Act 1986 and the National Centre for the 3Rs' *Responsibility in the Use of Animals for Medical Research* (2019). Random-bred CD1 embryos were collected from pregnant females between embryonic days (E) 10.5 and 14.5 (E0.5 is the day of finding a copulation plug). Embryos were dissected in Dulbecco's modified Eagle's Medium (DMEM), rinsed in PBS, and fixed in 4% PFA overnight.

Embryo measurements

Measurements on human embryos were made post-fixation using an eyepiece graticule on a Zeiss SV6 stereo microscope. Crown-rump length was measured as the maximum distance from the top of the head to the base of the spine. Tail length was measured along the ventral surface, from the tail tip to the point where the tail joined the trunk. The distance from the tail tip to the caudal edge of the caudal-most somite was also measured. Somites were counted in total or, where indistinct more rostrally, the total number was estimated by considering the somite immediately rostral to the hindlimb bud as somite 24. Analysis of PNP closure by somite stage (Figure 1I,J) was performed using archival embryo images, with PNP length measurements normalised to caudal somite length in the same embryo (both measured in pixels on photomicrographs).

Embryo sections

PFA-fixed caudal embryonic regions were dissected away from the remainder of the embryo and processed for paraffin wax histology. Tissues were dehydrated through an ascending alcohol series to Histoclear (National Diagnostics), embedded in 56°C paraffin wax, and sectioned transversely at 7 µm thickness on a rotary microtome. Sections were processed either for haematoxylin and eosin staining, or for immunohistochemistry, as described below.

Immunohistochemistry for apoptosis and cell proliferation

Primary antibodies for immunohistochemistry were: (i) anti-cleaved caspase-3 (Asp175; Cell Signaling, Cat. No. 9661) at a dilution of 1:1000; (ii) anti-phosphohistone-H3 (Upstate, Cat. No. 06-755) at a dilution of 1: 400. Staining was according to manufacturer's instructions except that Declere (Cell Marque, Cat. No. 921P) was used instead of xylene and ethanol, to dewax and rehydrate the sections. TdT-mediated dUTP-biotin nick end labelling (TUNEL; Apoptag) was performed according to manufacturer's instructions. Sections were counterstained with methyl green (Vector Labs, H-3402) .

Whole mount in situ hybridisation

Digoxygenin (DIG)-labelled mRNA probes for human *FGF8* (reference sequence NM_033165.5) and *WNT3A* (reference sequence NM_033131.4) were designed for *in situ* hybridisation. Human embryos or isolated caudal regions were fixed in 10% formalin, washed in phosphate buffered saline with 0.1% Tween (PBT), and processed for whole mount *in situ* hybridisation. Samples were bleached in 6% hydrogen peroxide, digested in a 5 µg/ml proteinase K - PBT solution, followed by a wash in 2 mg/ml glycine, and subsequently fixed in 0.2% glutaraldehyde made up in 4% paraformaldehyde. Samples were then incubated in pre-hybridisation mix (composed of 50% formamide, 1% sodium dodecyl sulfate (SDS), 5x saline sodium citrate (SSC), 50 µg/ml yeast tRNA and 50 µg/ml heparin), and hybridised with the corresponding digoxigenin (DIG)-labelled mRNA probes overnight at 70 °C. Hybridised probes were fixed using fixative wash solutions

(solution 1 comprising 50% formamide, 5x SSC and 1% SDS at 70 °C; and solution 2 comprising 50% formamide, 2x SSC and 1% SDS at 65 °C). The samples were then blocked in 10% heat inactivated sheep serum, and incubated with anti-DIG-alkaline phosphatase antibody (Roche) solution. Developmental of the colour signal was carried out using nitrotetrazolium blue (NBT) and 5-bromo-4-chloro-3-indole (BCIP) solution. Whole mount images were taken using a DFC490 camera (Leica) connected to a Stemi SV11 stereomicroscope (Zeiss), and then embedded in gelatin-albumin blocks for vibratome sectioning at a thickness of 40 μm. Sections were imaged using bright field light transmission and AxioVision v4.8.2 software on an Axioplan 2 microscope (Zeiss).

Acknowledgements

This work was supported in part by the Wellcome Human Developmental Biology Initiative (HDBI: grant 215116/Z/18/Z). Human embryonic material was provided by the MRC/Wellcome Human Developmental Biology Resource (grant MR/R006237/1; www.hdbr.org).

Table 1. Number of human embryos in the study, with breakdown by sex and method of pregnancy termination *

Analysis type	Figures in paper	Total no.	No. females	No. males	No. sex unknown	No. medical	No. surgical
PNP morphology	1A-H	2 **	0	2	0	2	0
PNP closure timing	1I,J	40	24	16	0	40	0
Histology, cell death	2-4	37 **	14	21	2	36	1
FGF8, WNT3A expr.	5-6	18	9	9	0	18	0
Serial section analysis	7	5	3	1	1	4	1
Totals		102	50	49	3	100	2

* Medical: mifepristone- and misoprostol-induced delivery; Surgical: ultrasound-guided vacuum aspiration.

** Embryos included in Table 2

Table 2. Measurements of human embryos, CS12-18 *

Carnegie Stage (CS)	Age range (days post-fertilization)	Number of embryos	Somite number **	Crown-rump length ***	Tail length (total) ***	Tail length distal to somites ***
12	25-27	2	22, 22	3.0, 3.0	N/A	N/A
13	28-30	7	35.4 ± 2.3	6.4 ± 1.3	1.06 ± 0.44	0.49 ± 0.16
14	31-32	5	35.0 ± 2.0	8.4 ± 2.2	0.99 ± 0.21	0.56 ± 0.06
15	33-35	7	35.9 ± 1.8	8.9 ± 0.8	1.18 ± 0.55	0.67 ± 0.15
16	37-39	8	36.6 ± 1.2	11. 7 ± 1.2	1.29 ± 0.48	0.46 ± 0.13
17	40-43	4	32.3 ± 2.1	12.2 ± 1.2	1.18 ± 0.20	0.34 ± 0.01
18	44-45	6	32.6 ± 1.1	15.4 ± 2.2	1.14 ± 0.48	N/D

* Embryos that contributed to Figure 1A-H (CS12) and Figures 2-4 (CS13-18)

** Somite numbers: mean ± SD (except CS12, where actual somite numbers are shown)

*** Lengths (mm): mean ± SD (except CS12, where actual lengths are shown)

N/A: not applicable; N/D: not determined

REFERENCES

Agarwalla PK, Dunn IF, Scott RM, Smith ER. (2007) **Tethered cord syndrome** *Neurosurg Clin N Am*. **18**:531-547.

Amadei G, Handford CE, Qiu C, De Jonghe J, Greenfeld H, Tran M, Martin BK, Chen DY, Aguilera-Castrejon A, Hanna JH, Elowitz MB, Hollfelder F, Shendure J, Glover DM, Zernicka-Goetz M. (2022) **Embryo model completes gastrulation to neurulation and organogenesis** *Nature*. **610**:143-153.

Bolli R. (1966) **Sekundäre lumenbildungen im neuralrohr und rückenmark menschlicher embryonen** *Acta Anat*. **64**:48-81.

Bullen P, Wilson DI. (1997) **The carnegie staging of human embryos: A practical guide** In: Strachan T, Lindsay S, Wilson DI, editors. Molecular genetics of early human development. Oxford: BIOS Scientific Publishers Ltd. p. 27-50.

Butcher EO. (1929) **The development of the somites in the white rat (mus norvegicus albinus) and the fate of the myotomes, neural tube and gut in the tail** *Am J Anat*. **44**:381-439.

Cambray N, Wilson V. (2002) **Axial progenitors with extensive potency are localised to the mouse chordoneural hinge** *Development*. **129**:4855-4866.

Cambray N, Wilson V. (2007) **Two distinct sources for a population of maturing axial progenitors** *Development*. **134**:2829-2840.

Catala M. (2021) **Overview of secondary neurulation** *J Korean Neurosurg Soc*. **64**:346-358.

Cogliatti SB. (1986) **Diplomyelia: Caudal duplication of the neural tube in mice** *Teratology*. **34**:343-352.

Copp AJ, Adzick NS, Chitty LS, Fletcher JM, Holmbeck GN, Shaw GM. (2015) **Spina bifida** *Nat Rev Dis Primers*. **1**:15007.

Copp AJ, Seller MJ, Polani PE. (1982) **Neural tube development in mutant (curly tail) and normal mouse embryos: The timing of posterior neuropore closure in vivo and in vitro** *J Embryol Exp Morphol*. **69**:151-167.

Criley BB. (1969) **Analysis of the embryonic sources and mechanisms of development of posterior levels of chick neural tubes** *J Morph*. **128**:465-501.

Denham M, Hasegawa K, Menheniott T, Rollo B, Zhang D, Hough S, Alshawaf A, Febbraro F, Ighaniyan S, Leung J, Elliott DA, Newgreen DF, Pera MF, Dottori M. (2015) **Multipotent caudal neural progenitors derived from human pluripotent stem cells that give rise to lineages of the central and peripheral nervous system** *Stem Cells*. **33**:1759-1770.

Diaz-Cuadros M, Wagner DE, Budjan C, Hubaud A, Tarazona OA, Donelly S, Michaut A, Al Tanoury Z, Yoshioka-Kobayashi K, Niino Y, Kageyama R, Miyawaki A, Touboul J, Pourquie

O. (2020) **In vitro characterization of the human segmentation clock** *Nature*. **580**:113-118.

Fallon JF, Simandl BK. (1978) **Evidence of a role for cell death in the disappearance of the embryonic human tail** *Am J Anat*. **152**:111-129.

Fedorova V, Vanova T, Elrefae L, Pospisil J, Petrasova M, Kolajova V, Hudacova Z, Baniariova J, Barak M, Peskova L, Barta T, Kaucka M, Killinger M, Vecera J, Bernatik O, Cajanek L, Hribkova H, Bohaciakova D. (2019) **Differentiation of neural rosettes from human pluripotent stem cells in vitro is sequentially regulated on a molecular level and accomplished by the mechanism reminiscent of secondary neurulation** *Stem Cell Res*. **40**:101563.

Gajovic S, Kostovic-Knezevic L, Svajger A. (1989) **Origin of the notochord in the rat embryo tail** *Anat Embryol*. **179**:305-310.

Gajovic S, Kostovic-Knezevic L, Svajger A. (1993) **Morphological evidence for secondary formation of the tail gut in the rat embryo** *Anat Embryol (Berl)*. **187**:291-297.

Gonzalez-Gobartt E, Blanco-Ameijeiras J, Usieto S, Allio G, Benazeraf B, Marti E. (2021) **Cell intercalation driven by smad3 underlies secondary neural tube formation** *Dev Cell*. **56**:1147-1163 e1146.

Henrique D, Abranches E, Verrier L, Storey KG. (2015) **Neuromesodermal progenitors and the making of the spinal cord** *Development*. **142**:2864-2875.

Hughes AF, Freeman RB. (1974) **Comparative remarks on the development of the tail cord among higher vertebrates** *J Embryol Exp Morphol*. **32**:355-363.

Jolly J, Ferester-Tadie M. (1936) **Recherches sur l'oeuf du rat et de la souris** *Arch d'Anat Microsc*. **32**:323-390.

Jones VJ, Greene NDE, Copp AJ. (2019) **Genetics and developmental biology of closed dysraphic conditions** In: Tubbs RS, Oskouian RJ, Blount JP, Oakes WJ, editors. Occult spinal dysraphism. Springer. p. 325-344.

Karzbrun E, Khankhel AH, Megale HC, Glasauer SMK, Wyle Y, Britton G, Warmflash A, Kosik KS, Siggia ED, Shraiman BI, Streichan SJ. (2021) **Human neural tube morphogenesis in vitro by geometric constraints** *Nature*. **599**:268-272.

Kostovic-Knezevic L, Gajovic S, Svajger A. (1991) **Morphogenetic features in the tail region of the rat embryo** *Int J Dev Biol*. **35**:191-195.

Krupp DR, Xu PT, Thomas S, Dellinger A, Etchevers HC, Vekemans M, Gilbert JR, Speer MC, Ashley-Koch AE, Gregory SG. (2012) **Transcriptome profiling of genes involved in neural tube closure during human embryonic development using long serial analysis of gene expression (long-sage)** *Birth Defects Res A Clin Mol Teratol*. **94**:683-692.

Kunitomo K. (1918) **The development and reduction of the tail and of the caudal end of the spinal cord** *Carnegie Inst Contr Embryol*. **8**:161-198.

Lemire RJ. (1969) **Variations in development of the caudal neural tube in human embryos (horizons xiv-xxi)** *Teratology*. **2**:361-370.

Libby ARG, Joy DA, Elder NH, Bulger EA, Krakora MZ, Gaylord EA, Mendoza-Camacho F, Butts JC, McDevitt TC. (2021) **Axial elongation of caudalized human organoids mimics aspects of neural tube development** *Development*. **148**:dev 198275.

Matsuda M, Yamanaka Y, Uemura M, Osawa M, Saito MK, Nagahashi A, Nishio M, Guo L, Ikegawa S, Sakurai S, Kihara S, Maurissen TL, Nakamura M, Matsumoto T, Yoshitomi H, Ikeya M, Kawakami N, Yamamoto T, Woltjen K, Ebisuya M, Toguchida J, Alev C. (2020) **Recapitulating the human segmentation clock with pluripotent stem cells** *Nature*. **580**:124-129.

McShane SG, Mole MA, Savery D, Greene ND, Tam PP, Copp AJ. (2015) **Cellular basis of neuroepithelial bending during mouse spinal neural tube closure** *Dev Biol*. **404**:113-124.

Miller SA, Briglin A. (1996) **Apoptosis removes chick embryo tail gut and remnant of the primitive streak** *Dev Dyn*. **206**:212-218.

Moris N, Anlas K, van den Brink SC, Alemany A, Schroder J, Ghimire S, Balayo T, van Oudenaarden A, Martinez Arias A. (2020) **An in vitro model of early anteroposterior organization during human development** *Nature*. **582**:410-415.

Müller F, O'Rahilly R. (1987) **The development of the human brain, the closure of the caudal neuropore, and the beginning of secondary neurulation at stage 12** *Anat Embryol*. **176**:413-430.

Müller F, O'Rahilly R. (2004) **The primitive streak, the caudal eminence and related structures in staged human embryos** *Cells Tissues Organs*. **177**:2-20.

Nievelstein RAJ, Hartwig NG, Vermeij-Keers C, Valk J. (1993) **Embryonic development of the mammalian caudal neural tube** *Teratology*. **48**:21-31.

O'Rahilly R, Muller F. (1987) **Developmental stages in human embryos**. Washington: Carnegie Institute of Washington, Publication 637.

O'Rahilly R, Müller F. (2002) **The two sites of fusion of the neural folds and the two neuropores in the human embryo** *Teratology*. **65**:162-170.

Olivera-Martinez I, Harada H, Halley PA, Storey KG. (2012) **Loss of fgf-dependent mesoderm identity and rise of endogenous retinoid signalling determine cessation of body axis elongation** *PLoS Biol*. **10**:e1001415.

Pang D. (2020) **Perspectives on spinal dysraphism : Past, present, and future** *J Korean Neurosurg Soc*. **63**:366-372.

Pytel A, Bruska M, Wozniak W. (2007) **Evidence that the caudal portion of the neural tube develops by cavitation of a neural cord in the caudal eminence of human embryos** *Folia Morphol (Warsz)*. **66**:104-108.

Qi BQ, Beasley SW, Williams AK, Fizelle F. (2000) **Apoptosis during regression of the tailgut and septation of the cloaca** *J Pediatr Surg*. **35**:1556-1561.

Rifes P, Isaksson M, Rathore GS, Aldrin-Kirk P, Moller OK, Barzaghi G, Lee J, Egerod KL, Rausch DM, Parmar M, Pers TH, Laurell T, Kirkeby A. (2020) **Modeling neural tube development by differentiation of human embryonic stem cells in a microfluidic wnt gradient** *Nat Biotechnol*. **38**:1265-1273.

Saitsu H, Yamada S, Uwabe C, Ishibashi M, Shiota K. (2004) **Development of the posterior neural tube in human embryos** *Anat Embryol (Berl)*. **209**:107-117.

Sapunar D, Vilovic K, England M, Saraga-Babic M. (2001) **Morphological diversity of dying cells during regression of the human tail** *Ann Anat*. **183**:217-222.

Schoenwolf GC. (1984) **Histological and ultrastructural studies of secondary neurulation of mouse embryos** *Am J Anat*. **169**:361-374.

Schoenwolf GC, De Longo J. (1980) **Ultrastructure of secondary neurulation in the chick embryo** *Am J Anat*. **158**:43-63.

Shum ASW, Copp AJ. (1996) **Regional differences in morphogenesis of the neuroepithelium suggest multiple mechanisms of spinal neurulation in the mouse** *Anat Embryol*. **194**:65-73.

Streeter GL. (1919) **Factors involved in the formation of the filum terminale** *Am J Anat*. **25**:1-11.

Svajger A, Kostovic-Knezevic L, Bradamante Z, Wrischer M. (1985) **Tail gut formation in the rat embryo** *Roux's Arch Dev Biol*. **194**:429-432.

Tam PPL. (1984) **The histogenetic capacity of tissues in the caudal end of the embryonic axis of the mouse** *J Embryol Exp Morphol*. **82**:253-266.

Tojima S, Makishima H, Takakuwa T, Yamada S. (2018) **Tail reduction process during human embryonic development** *J Anat*. **232**:806-811.

Tzouanacou E, Wegener A, Wymeersch FJ, Wilson V, Nicolas JF. (2009) **Redefining the progression of lineage segregations during mammalian embryogenesis by clonal analysis** *Dev Cell*. **17**:365-376.

Vilovic K, Ilijic E, Glamoclija V, Kolic K, Bocina I, Sapunar D, Saraga-Babic M. (2006) **Cell death in developing human spinal cord** *Anatomy and Embryology*. **211**:1-9.

Wilson V, Olivera-Martinez I, Storey KG. (2009) **Stem cells, signals and vertebrate body axis extension** *Development*. **136**:1591-1604.

Wymeersch FJ, Wilson V, Tsakiridis A. (2021) **Understanding axial progenitor biology in vivo and in vitro** *Development*. **148**:dev.180612.

Yang HJ, Lee DH, Lee YJ, Chi JG, Lee JY, Phi JH, Kim SK, Cho BK, Wang KC. (2014) **Secondary neurulation of human embryos: Morphological changes and the expression of neuronal antigens** *Childs Nerv Syst*. **30**:73-82.

Yang HJ, Wang KC, Chi JG, Lee MS, Lee YJ, Kim SK, Cho BK. (2003) **Neural differentiation of caudal cell mass (secondary neurulation) in chick embryos: Hamburger and hamilton stages 16-45** *Developmental Brain Research*. **142**:31-36.

Santos et al - Figures 1-7

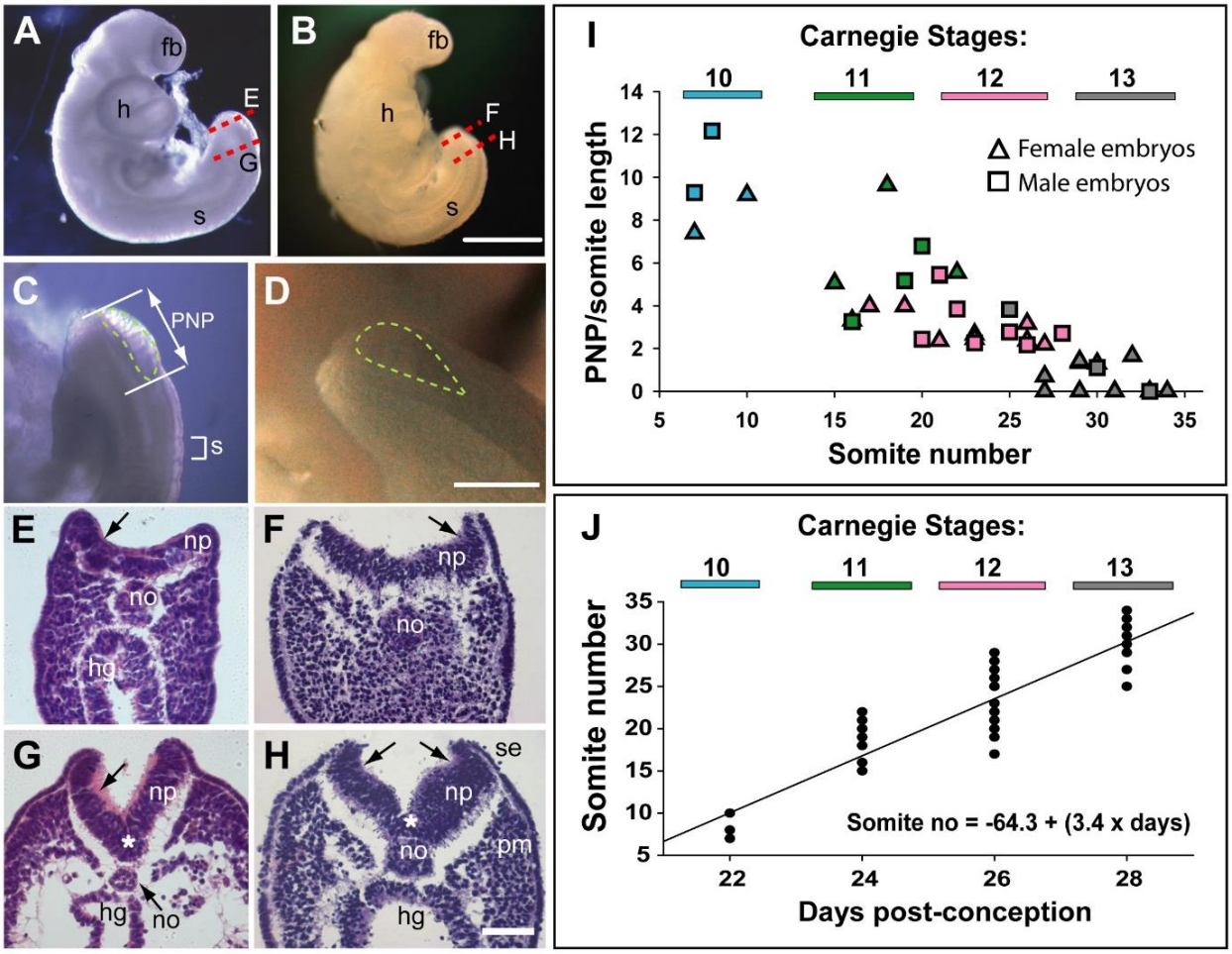

Figure 1. Morphology and timing of human posterior neuropore (PNP) closure. (**A, B**) Two CS12 embryos viewed from right side, each with 22-23 somites (s), and a looped heart (h). Neural tube closure is complete along most of the body axis, including the forebrain (fb), whereas the PNP remains open caudally. (**C, D**) Magnified oblique views from upper right side of the caudal region; the open PNP is outlined with dashed lines. (**E-H**) H&E-stained transverse sections, through the PNP, with section planes as indicated by dashed lines in A, B. The most caudally located sections (E, F) show a relatively flat neural plate (np), although incipient dorsolateral hinge points (DLHPs; arrows) are visible. Note the midline notochord (no) underlying the neural plate, and hindgut (hg) beneath the notochord (in E only). More rostral sections (G, H) show elevated neural folds with DLHPs clearly visible (arrows: unilateral in G, bilateral in H), located where basal contact of the neural plate changes from surface ectoderm (se), to paraxial mesoderm (pm). A median hinge point (MHP; asterisks in G, H) overlies the notochord. (**I**) PNP length (double headed arrow in C), normalised to somite (s) length (bracketed in C), determined from photographic images of 40 human embryos (24

females; 16 males) at CS10 (n = 4), CS11 (n = 8), CS12 (n = 16) and CS13 (n = 12). Symbol colours indicate the Carnegie Stages assigned at the time of collection. The PNP shows gradual closure, with completion around the 30 somite stage. (**J**) Somite number of the 40 embryos in I, plotted against days post-conception for each Carnegie Stage. The linear regression equation is shown, with $R^2 = 0.82$, and $p < 0.001$. Scale bars: 1 mm in A, B; 0.4 mm in C, D; 0.1 mm in E-H.

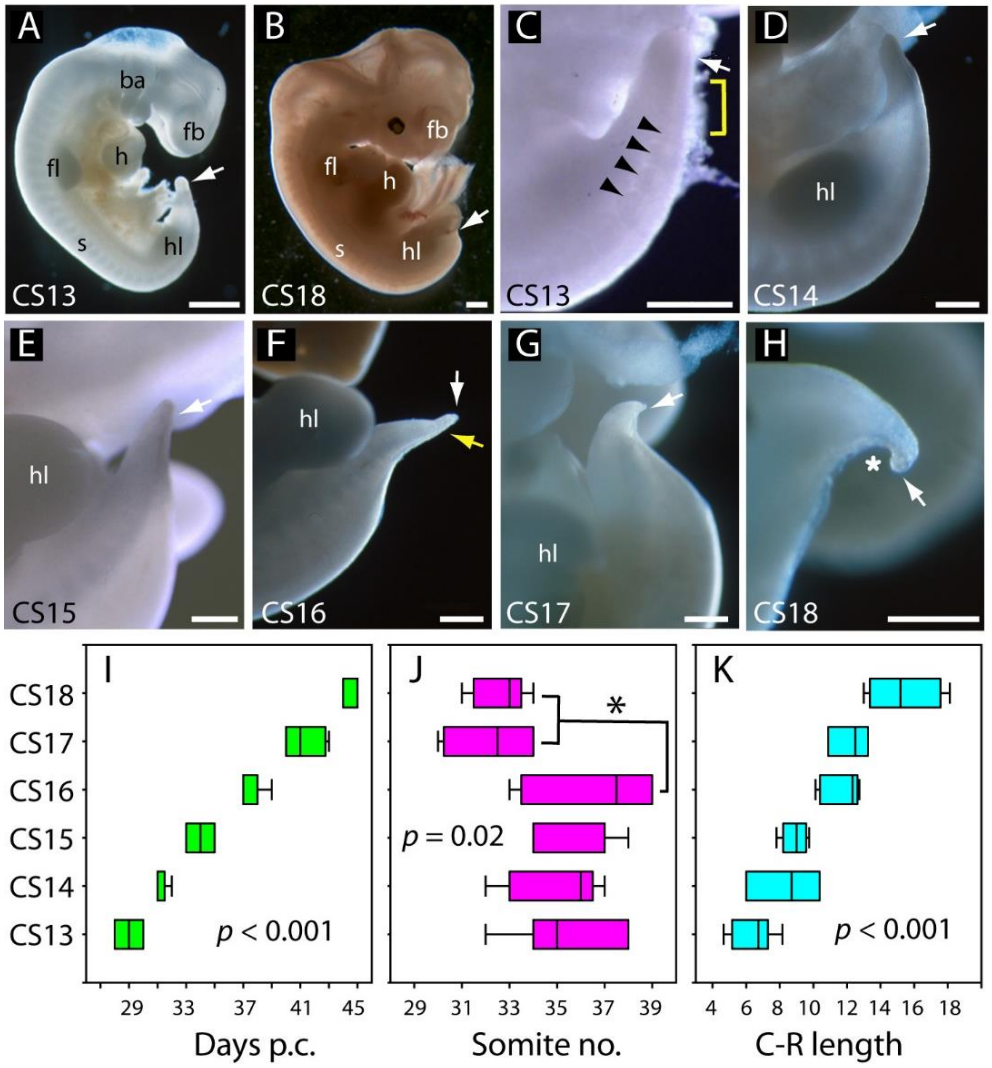

Figure 2. Development of the tail in human embryos. (**A, B**) Whole embryos at CS13 (A) and CS18 (B), showing the range of stages studied (4-6.5 weeks post-conception). The tail bud (arrow) is well formed at CS13 following completion of PNP closure at CS12, whereas, by CS18, tail development and regression are largely complete and only a small tail remnant remains (arrow). (**C-H**) Higher magnification views of the caudal region at CS13 to CS18. At CS13, the tail bud is relatively massive, tapering gradually and with a rounded end (arrow in C). Somites are visible rostral to the tail bud (arrowheads) with an intervening region of presomitic mesoderm (yellow bracket). At CS14 and CS15 the tail narrows progressively,

with distal tapering (arrows in D-E). By CS16, this has yielded a slender structure with narrow pointed end (white arrow in F) in which somites extend almost to the tail tip (yellow arrow in F). Thereafter, the tail shortens progressively (arrows in G, H), develops a marked flexion (asterisk in H), and becomes increasingly transparent (G, H). (**I-K**) Analysis of embryos in the range CS13-CS16 (Table 2), plotting CS against: (I) days post-conception (p.c.), (J) somite no. and (K) crown-rump (C-R) length in mm. One-way ANOVA on ranks shows all three parameters vary significantly with CS (*p*-values on graphs). Somite no. reduces significantly between CS16 and CS17/18 (* $p < 0.05$). Abbreviations: ba, branchial arches; fb, forebrain; fl, forelimb; h, heart; hl, hindlimb; s, somites. Scale bars: 1 mm in A, B; 0.5 mm in C-H.

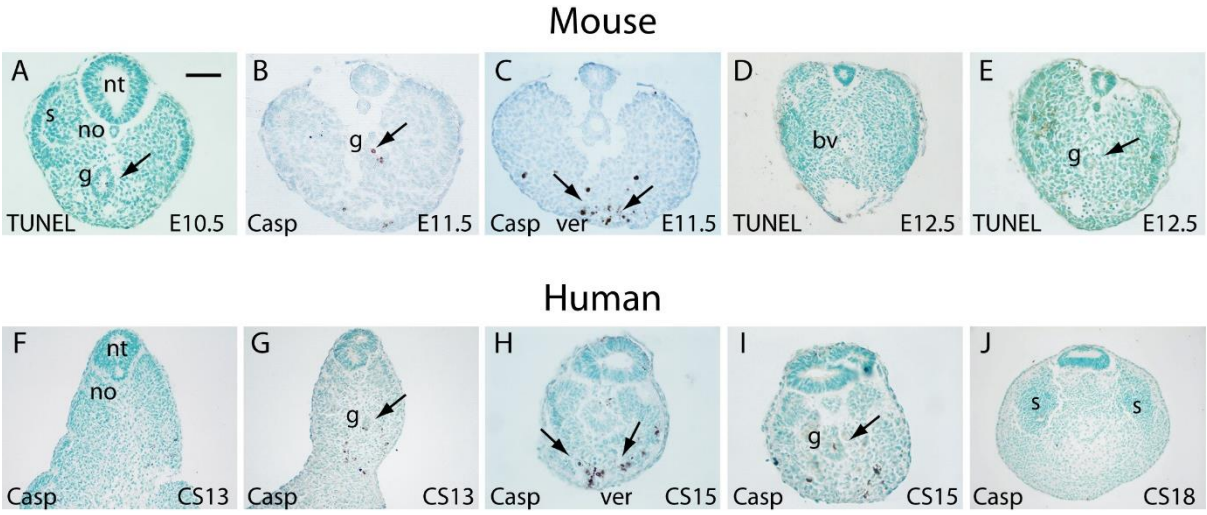

Figure 3. Programmed cell death during regression of tail structures in mouse and human embryos. Transverse sections through the tail region of mouse (A-E) and human (F-J) embryos at the stages indicated on the panels. Staining is by TUNEL method (A, D, E) or using an antibody specific for activated caspase 3 (B, C, F-J), with counterstaining by methyl green. Particularly intense programmed cell death (PCD) is observed in the ventral midline mesoderm overlying the ventral ectodermal ridge (ver) of both species (arrows in C, H). PCD can also be detected in the tail-gut (g) of both mouse and human embryos (arrows in A, B, G, I). Significantly, the tail-gut can be clearly identified in a caudal section through an E12.5 mouse tail (arrow in E), whereas it is absent from a more rostral section of the same tail (D). A blood vessel (bv) can be seen where the gut was previously situated in this section. Similarly, in a CS13 human embryo, the tail-gut is absent from a rostral section (F) but present more caudally in the same embryonic tail, with dying cells visible in the distal tail-gut remnant (arrowhead in G). Hence, tail-gut regression proceeds in a rostral to caudal direction in both

species. Other abbreviations: no, notochord; nt, neural tube. Scale bar in A represents: 50 µm (A,H,I), 70 µm (B,C,F,G) and 80 µm (D,E,J).

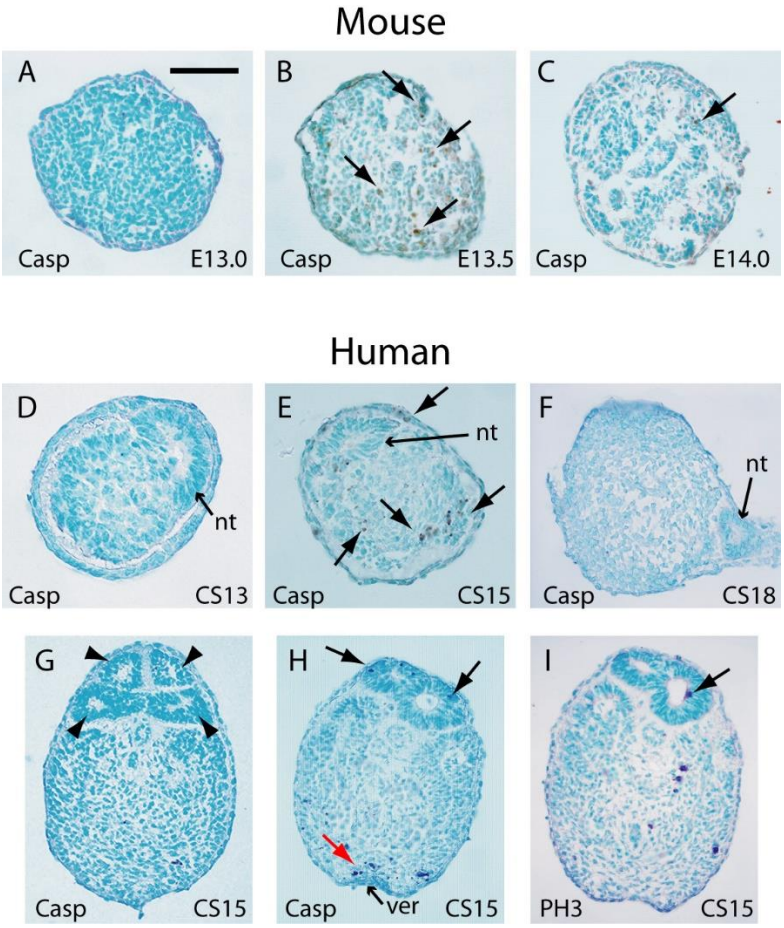

Figure 4. Stage-dependent cell death and multiple neural tube lumens in mouse and human tails. Transverse sections through the tails of mouse (A-C) and human (D-I) embryos stained with antibodies to activated caspase 3 antibody (A-H; Casp) or phospho-histone H3 (I; PH3). Developmental stages are indicated on the panels. (**A-C**) In mouse embryos, the tail bud displays a stage-dependent burst of PCD at E13.5 (arrows in B), with absence of caspase 3-positive cells 12 hours earlier, at E13.0 (A), and only occasional dying cells 12 hours later, at E14.0 (arrow in C). Note the absence of a neural tube in the mouse tail bud tip, and the sparse nature of the tail bud mesenchyme at E14.0. (**D-F**) Human embryonic tail buds show a similar developmental sequence to the mouse, with absence of PCD at CS13 (D), abundant dying cells at CS15 (arrows in E) and cessation of PCD by CS18 (F). Unlike the mouse, the secondary neural tube extends to the tail bud tip (nt in D-F), with this terminal neural tube portion having a single lumen in all three embryos. (**G-I**). Multiple neural tube profiles were observed in 9/15 human tails, with variability in the number of lumens: four lumens are visible in one CS15 embryo (arrowheads in G) but only two in sections of a second embryo of the same stage (H,I). Adjacent sections through this second human embryonic tail demonstrate

both PCD (arrows in H) and mitotic activity (arrow in I) occurring simultaneously in the secondary neural tube, whereas the mesenchyme overlying the ventral ectodermal ridge (ver) exhibits plentiful PCD (red arrow in H), but no mitotic activity (I). Scale bar in A represents: 50 µm in A-C, F-I and 30 µm in D,E.

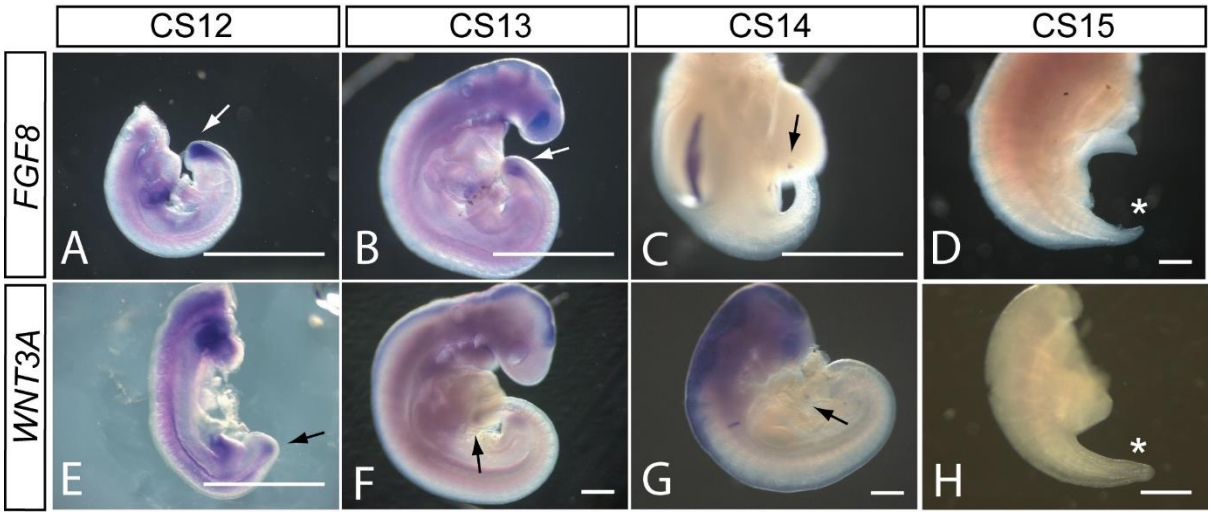

Figure 5. FGF8 and WNT3A expression in the elongating caudal region of human embryos. Whole mount *in situ* hybridisation for *FGF8* (A-D) and *WNT3A* (E-H) in embryos at CS12 (A, E), CS13 (B, F), CS14 (C, G) and CS15 (D, H). Both genes show prominent expression domains in the tail bud at CS12 when axial elongation is underway and the posterior neuropore (PNP) is closing (arrows in A, E). At CS13, following PNP closure, expression of *FGF8* and *WNT3A* remains prominent although less intense and more localised to the terminal tail bud than at CS12 (arrows in B, F). By CS14, both genes exhibit much smaller, high localised expression domains that each appears as a 'dot' within the tail bud region (arrows in C, G). By CS15, axial elongation has ceased, the tail tip has narrowed and is increasingly transparent. At this stage, expression of neither gene can be detected (asterisks in D, H). Note that whole embryos are shown in B, F, G while isolated trunk/caudal regions are shown in A, C, D, E, H. No. embryos analysed: FGF8, n = 2 for each stage; WNT3A, n = 2 for each stage except n = 3 for CS13. Scale bars: 500 µm.

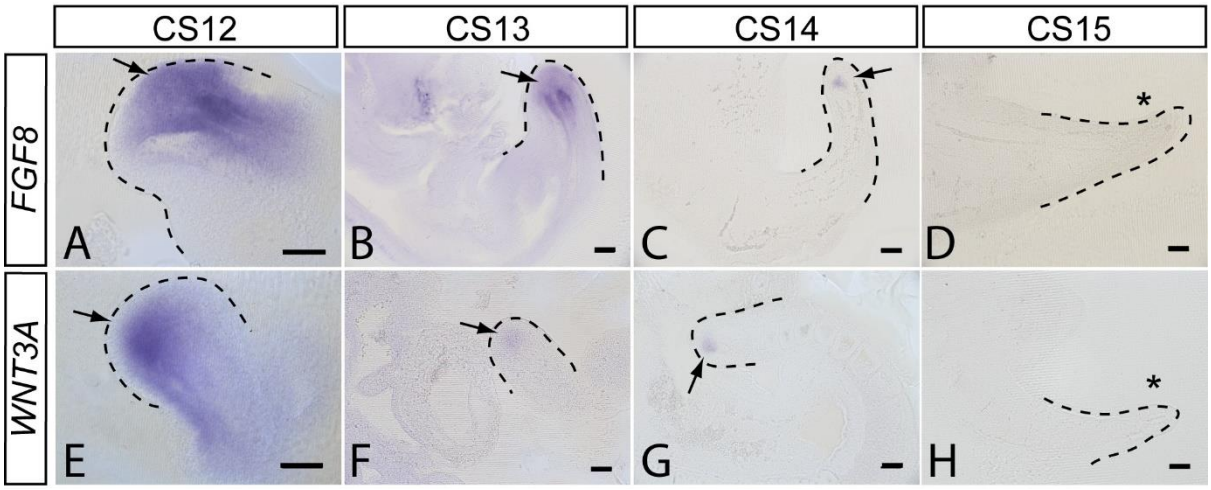

Figure 6. FGF8 and WNT3A expression in sections through the elongating caudal region of human embryos. Vibratome sections with sagittal orientation of the whole mount *in situ* hybridisation embryos shown in Fig 5. Expression of *FGF8* (A-D) and *WNT3A* (E-H) is shown in embryos at CS12 (A, E), CS13 (B, F), CS14 (C, G) and CS15 (D, H). Tail bud region is outlined by dotted lines. Extensive expression domains are visible for both *FGF8* and *WNT3A* at CS12 (A, E) whereas at CS13 (B, F) both genes are less intensely expressed, with transcripts for *WNT3A* particularly reduced compared with CS12. At CS14, only a small 'dot' of remaining expression is visible close to the tail bud tip for each gene. At CS15, no *FGF8* or *WNT3A* expression is detectable in the caudal region. No. embryos analysed: FGF8, n = 2 for each stage; WNT3A, n = 2 for each stage except n = 3 for CS13. Scale bars: 100 μm.

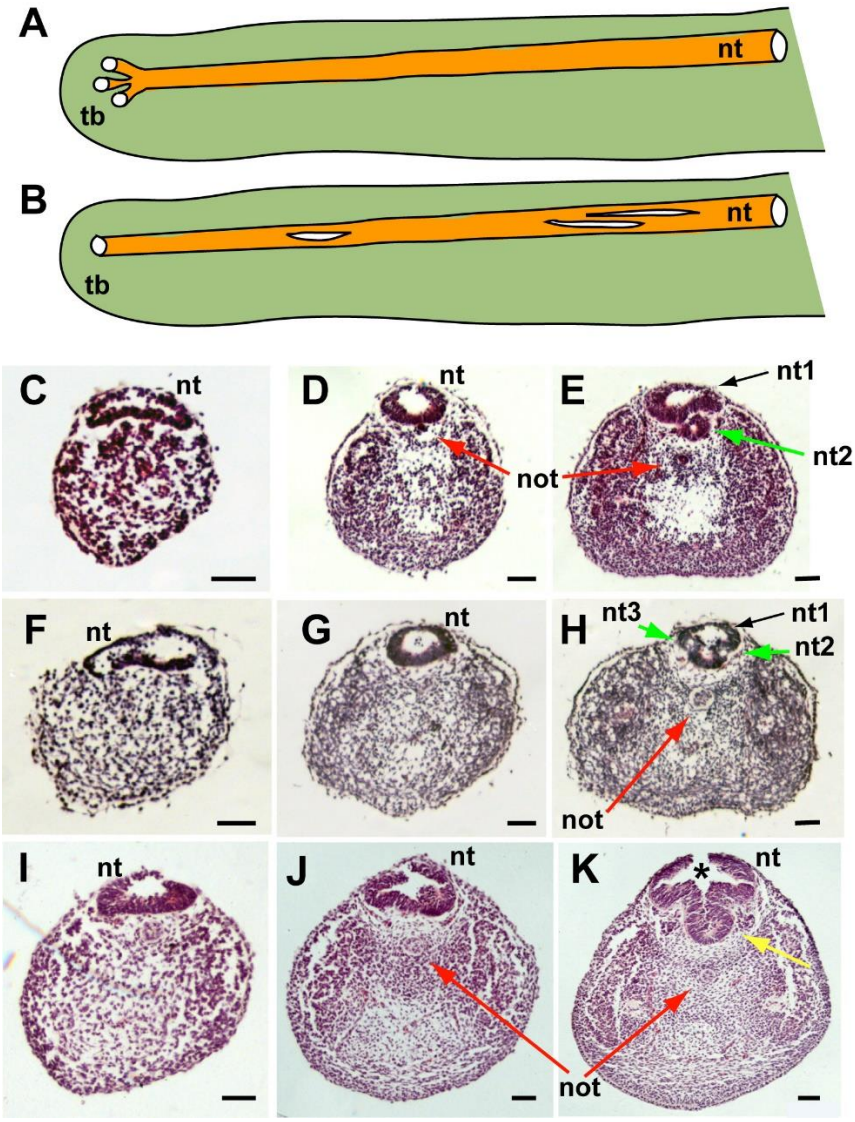

Figure 7. Mode of formation of the human secondary neural tube. (**A,B**) Two different hypotheses on the mode of human secondary neural tube (nt) formation. As in chick, it has been suggested that multiple lumens form initially in the tail bud (tb), and then coalesce to form the secondary neural tube (A). Alternatively, the finding of multiple neural tube lumens in sections of some human tails may reflect splitting of the secondary neural tube at more rostral levels (B). (**C-K**) Representative serial transverse sections (haematoxylin and eosin) through three different human embryonic tails at CS17 (C-E, F-H, I-K). Sections close to the tail bud tip (left side: C,F,I) show a broad, dorsoventrally flattened neural tube with a single lumen. There is no evidence of multiple lumens coalescing at such caudal levels in any embryos. Further rostrally (middle: D,G,J), sections show a neural tube with round profile and single lumen. Sections further rostrally in two embryos (right side: E,H) show evidence of secondary neural tube splitting, with two lumens (green arrows in E; nt1, nt2) and three lumens (green arrows in H; nt1, nt2, nt3). The third embryo shows a folded neural tube with ventral midline extension (yellow arrow in K) but only one lumen. Asterisk in K: dorsal gap in neural tube is a post-mortem artefact (also in J). Red arrows: secondary notochord (not). Scale bars: 50 µm.

Table S1. Publications on human secondary neural tube and body formation, showing topics covered

Study	Samples	PNP closure	Primary to secondary NT transition	Mode of secondary NT formation	Multiple NT lumens observed	Formation of secondary somites, notochord, tail-gut	Morphology of tail regression	Mode of cell death during regression	Gene expression
Kunitomo (1918). Carnegie Inst. Contr. Embryol 8, 161-198.	44 embryos, 4-125 mm crown-rump length, sections analysed from Carnegie collection		✓	✓	✓		✓		
Streeter (1919). Am. J. Anat. 25, 1-11.	Unspecified number of embryos, sections analysed from Carnegie collection			✓	✓		✓		
Bolli (1966). Acta. Anat. 64, 48-81.	123 normal embryos, 2-150 mm CRL, with unspecified method of collection			✓	✓		✓		
Lemire (1969). Teratology 2, 361-370.	8 embryos of CRL 6-25 mm, CS14-21, including from spontaneous abortions (3) and ectopic pregnancies (4)			✓	✓		✓	✓	
Hughes et al. (1974). J. Embryol. Exp. Morphol. 32, 355-363.	6 embryos at 28-40 days, sections analysed, with unspecified method of collection			✓	✓				
Fallon et al. (1978). Am. J. Anat. 152, 111-129.	52 embryos at CS14-22 from induced abortion			✓	✓		✓	✓	
Müller et al. (1987). Anat. Embryol. 176, 413-430.	24 embryos at CS12, sections analysed from Carnegie collection	✓	✓	✓		✓			
Müller et al. (1988). Anat. Embryol. (Berl) 177, 203-224.	25 embryos at CS13, sections analysed from Carnegie collection			✓	✓	✓			
Nievelstein et al. (1993). Teratology 48, 21-31.	36 embryos CS11-23 of unspecified origin	✓	✓	✓			✓	✓	
Saraga-Babic et al. (1994). Ann. Anat. 176, 277-286.	20 embryos at 4-12 weeks, obtained from artificial abortions			✓		✓	✓		✓
Saraga-Babic et al. (1995). J. Brain Res. 36, 341-347.	15 embryos aged 4-8 developmental weeks (CS12-23) from artificial abortions	✓	✓	✓	✓				
Peeters et al. (1998). Anat. Embryol. 198, 185-194.	11 embryos CS10-12, photographs analysed, of Kyto embryos from induced abortion for social reasons	✓							
Nakatsu et al. (2000). Anat. Embryol. (Berl) 201, 455-466.	68 normal embryos CS10-12 from pregnancy terminations for social reasons; a few from spontaneous or emergency abortions	✓							
Sapunar et al. (2001). Ann. Anat. 183, 217-222.	8 embryos at CS12-18 obtained from artificial abortions						✓	✓	
O'Rahilly et al. (2002). Teratology 65, 162-170.	98 embryos at CS8-13, sections analysed from Carnegie collection	✓							
Müller et al. (2004). Cells Tissues Organs 177, 2-20.	52 embryos at CS9-23, sections analysed from Carnegie collection	✓	✓	✓	✓	✓	✓		
Saitsu et al. (2004). Anat. Embryol. (Berl) 209, 107-117.	20 embryos around stage of posterior neuropore closure (CS12-13). Most from induced abortion for social reasons; one from ectopic pregnancy	✓	✓	✓	✓				

Vilovic et al. (2006). Anat. Embryol. 211, 1-9.	18 embryos at CS12-CS23 (5-12 weeks), from spontaneous or induced abortions						✓	✓	✓
Pytel et al. (2007). Folia Morphol. (Warsz.) 66, 104-108.	12 embryos at CS13-17, 32-41 days, with unspecified method of collection			✓	✓				
Saitsu et al. (2008). Congenit. Anom. (Kyoto) 48, 1-6.	43 embryos obtained from Kyoto collection from induced abortion for social reasons	✓	✓	✓	✓				
Krupp et al. (2012). Birth Defects Res. A Clin. Mol. Teratol. 94, 683-692.	8 or more CS12 and CS13 embryos, from mifepristone induced abortions								✓
Olivera-Martinez et al. (2012). PLoS Biol .10, e1001415.	3 embryos at CS12 (2) and CS16 (1) from induced abortion for social reasons				✓				✓
Yang et al. (2014). Childs Nerv. Syst. 30, 73-82.	21 embryos at CS12-23, from therapeutic pregnancy termination or surgical procedures to remove uterus/oviduct			✓	✓	✓	✓	✓	✓
Jang et al. (2016). Pediatr. Neurosurg. 51, 9-19.	20 embryos and fetuses, 6-14 weeks gestation from miscarriages and ectopic pregnancies		✓						
Tojima et al. (2018). J. Anat. 232, 806-811.	42 embryos at CS13-23 from Kyoto collection from induced abortion for social reasons					✓	✓		

Abbreviations: CS, Carnegie Stage; NT, neural tube; PNP, posterior neuropore